Salivary Gland Imaging

2

Jolie L. Chang

Key Points

1. Ultrasonography offers real-time, cost-effective images that can characterize salivary gland tumors, lymphadenopathy, sialolithiasis, and salivary duct obstruction and dilation. Ultrasound can further be used to target lesions for fine-needle aspiration biopsy.
2. Computed tomography is best used to evaluate salivary gland calcifications, bony erosion from tumors, and acute inflammation with concern for abscess formation.
3. Magnetic resonance imaging is the superior imaging modality for evaluating masses and tumors of the salivary glands due to excellent soft-tissue contrast and resolution. MRI can provide information about perineural invasion, tumor margins, extent of involvement in the parapharyngeal space, and lymph node metastasis.
4. Sialography provides detailed visualization of the main salivary duct and its branches within the gland parenchyma. Standard sialography involves cannulation of the major salivary duct papilla and infusion of contrast material. MR sialography is a newer technique that does not require contrast but has poorer spatial resolution.
5. Typical imaging findings for salivary gland lesions, tumors, autoimmune disease, sialolithiasis, and stenosis are discussed.

J.L. Chang, M.D.
Department of Otolaryngology—Head and Neck Surgery, University of California, San Francisco, 2380 Sutter Street, Box 0342, San Francisco, CA 94115, USA
e-mail: jolie.chang@ucsf.edu

Imaging Modalities

Conventional Radiography

Stones or calculi in the major salivary ducts can at times be visualized with conventional X-ray imaging. Attention to obtaining oblique lateral or occlusal views is required in order to visualize the region of the salivary ducts away from the bony facial skeleton. Historically, 80% of salivary calculi are radiopaque [1] on X-ray, and visualization depends on calcified content and stone size. CT imaging is more sensitive for detection and localization of small calcifications and has largely replaced conventional X-ray imaging for this purpose [2]. Despite this, routine dental imaging can uncover incidental calculi in the submandibular and parotid spaces. Soft-tissue lesions and tumors in the salivary glands are not adequately visualized with conventional X-ray.

Ultrasonography (US)

US is a real-time and cost-effective approach for initial imaging of many salivary gland disorders. US offers no radiation and provides targeted,

M.B. Gillespie et al. (eds.), *Gland-Preserving Salivary Surgery*,
https://doi.org/10.1007/978-3-319-58335-8_2

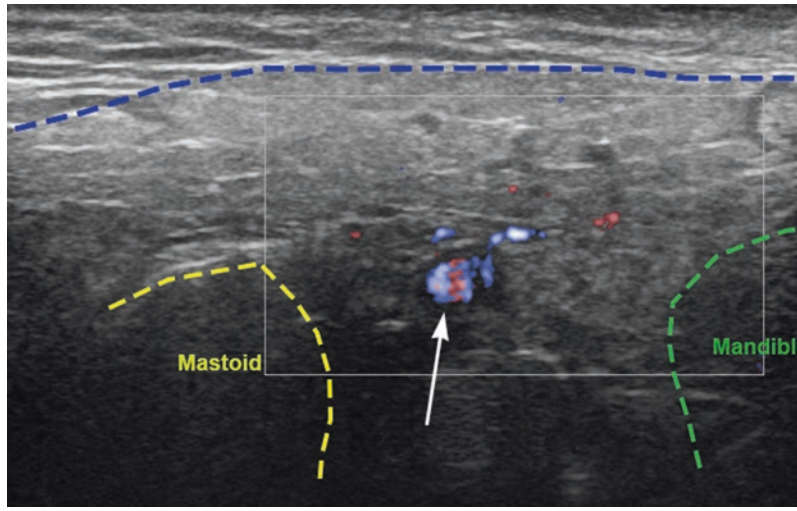

Fig. 2.1 Ultrasound image of the right parotid gland in the transverse plane outlines the superficial surface of the parotid (*blue dashed line*), the mastoid process (*yellow dashed line*), and the ramus of the mandible (*green dashed line*). The parotid gland is hyperechoic compared to surrounding tissue. The demarcation between superficial and deep lobes of the parotid is defined by the depth of the retromandibular vein (*white arrow*) which is visualized using Doppler

two-dimensional images of the head and neck using high-frequency linear array 7–15 MHz transducers. On exam, normal salivary glands are homogeneous and typically hyperechoic compared to surrounding muscle tissue due to higher fat content within the glands (Fig. 2.1).

Superficial tumors of the major salivary glands are easily imaged with US. The superficial lobe of the parotid is delineated from the deep lobe by the location of the facial nerve and its branches, which cannot be directly visualized on US. However, the facial nerve runs with the retromandibular vein. The retromandibular vein can be imaged and represents a marker for the relative depth and location of the facial nerve [3] (Fig. 2.1). For submandibular glands, most of the parenchyma except for the most superior extent can be evaluated using US. Salivary tumors on US should be assessed for size, shape, borders, and internal vascularity and content. Adjacent lymph nodes within the parotid gland and in the lateral neck can be assessed for size, shape, and signs of necrosis or metastasis. US cannot diagnose or definitively differentiate benign from malignant tumors; however, US can be used to target needle placement for fine-needle aspiration biopsies of salivary gland lesions.

For evaluation of the salivary duct system, the course of Stensen's and Wharton's ducts can be examined on US. The main parotid duct exits the hilum of the gland and courses superficial to the masseter muscle approximately 1 cm inferior to the zygomatic arch before piercing the buccinator muscle and entering the oral cavity opposite the second maxillary molar. An accessory parotid gland can be found in 20% of patients adjacent to the duct and projecting over the masseter [4] and should be examined for lesions. The submandibular duct exits the submandibular gland hilum and travels around the posterior edge of the mylohyoid muscle into the floor of mouth where it courses adjacent to the sublingual glands anteriorly to the papilla which opens in the anterior floor of mouth just lateral to the lingual frenulum. The normal, non-obstructed, salivary duct is not visible on US.

Obstructive disease from sialolithiasis or duct stenosis is suspected in patients who report recurrent periprandial swelling and pain of the gland. Intraductal obstruction from salivary duct stones or stenoses can lead to ductal dilation and allows the duct to be visualized on US (Fig. 2.2a). Calcifications in the ducts appear as hyperechoic smooth lesions with posterior acoustic shadow (Fig. 2.2b). US has the ability to provide precise,

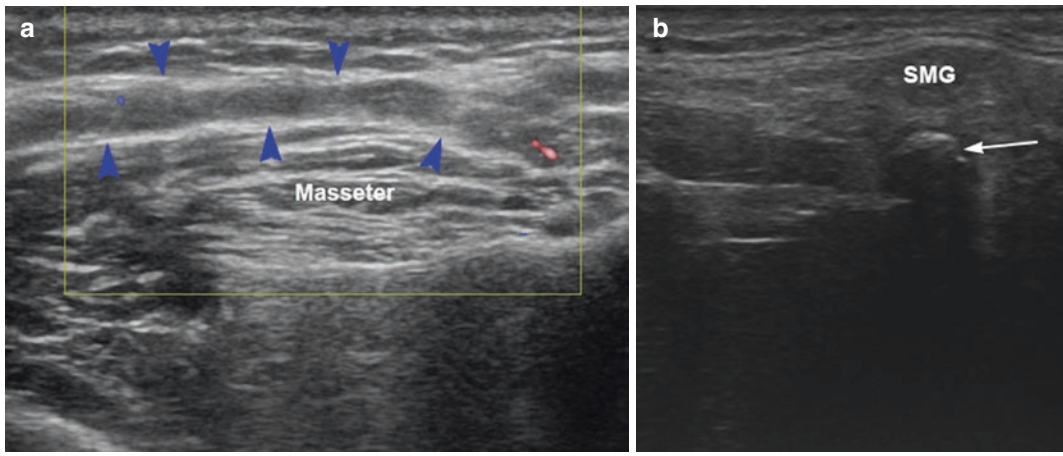

Fig. 2.2 Ultrasound of the left anterior cheek (**a**) demonstrates a dilated main parotid duct (*blue arrowheads*) over the masseter muscle due to distal stenosis at the papilla. The lack of Doppler flow within the hypoechoic tubular structure confirms the structure corresponds to a salivary duct. Ultrasound of the left submandibular gland hilum (**b**, SMG) reveals a hyperechoic calculus (*white arrow*) with posterior acoustic shadow

real-time localization of calculi which can be utilized intraoperatively to target surgical interventions. US has high sensitivity (94%) and specificity (100%) for detecting salivary calculi larger than 2 mm; smaller calculi do not routinely exhibit the posterior acoustic shadows [5]. Bimanual sono-palpation with digital palpation of the buccal mucosa for parotid ducts or the floor of mouth mucosa for submandibular ducts can be performed while applying external pressure with the ultrasound transducer and allows for visualization of the distal salivary ducts (Fig. 2.3). When a sialolith is large enough to cause significant duct obstruction, proximal duct dilation can be visualized as a hypoechoic tubular structure along the course of the salivary duct. The absence of color flow with Doppler confirms the identification of a salivary duct instead of a blood vessel (Fig. 2.2a). During the exam, patients with stenosis or obstruction can be given a sialogogue to stimulate saliva generation and promote visualization of a dilated duct.

US disadvantages include dependency on operator experience and technique. Images can be limited by incomplete visualization of the deep parotid lobe due to acoustic shadowing by the mandible. Similarly, pathology in the most anterior section of the floor of mouth can also be challenging to image. Large tumors in the parapharyngeal space may require multi-planar imaging for full assessment.

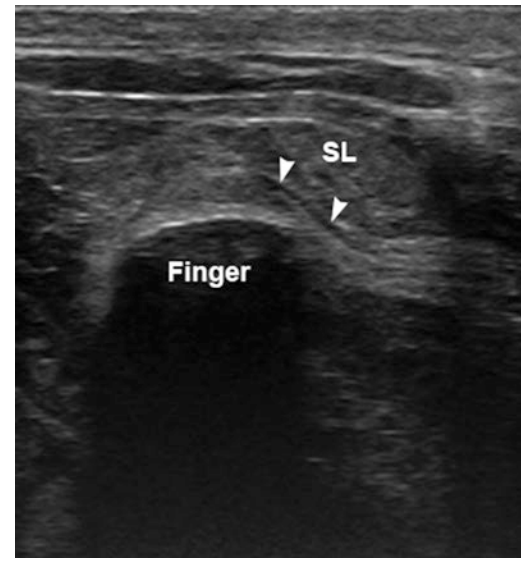

Fig. 2.3 Ultrasound of the left anterior submental space with bimanual sonopalpation with gloved finger in the anterior floor of mouth (finger) compressing the tissue against the US probe. A dilated submandibular duct (*arrowheads*) can be seen alongside sublingual tissue (SL)

Computed Tomography (CT)

CT is the imaging modality best suited to identify small calcifications in the salivary duct or gland and to evaluate for bony erosion from malignant neoplasms. Due to speed and accessibility, CT images are also best for evaluating acute inflammation

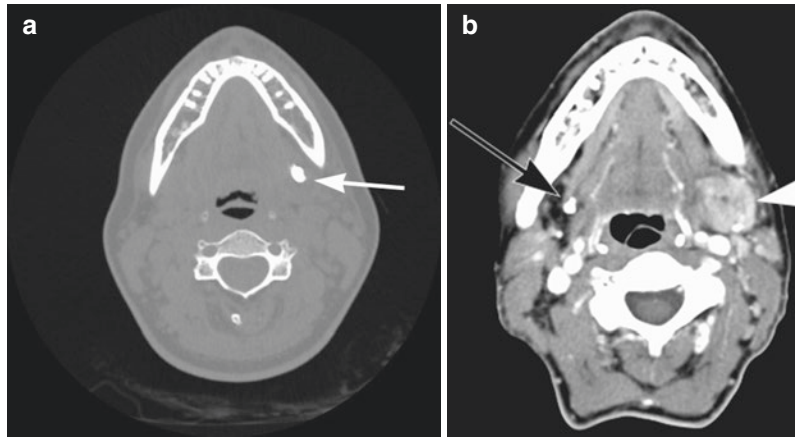

Fig. 2.4 CT scan without contrast (**a**) with left submandibular calculus at the hilum of the gland (*white arrow*). A patient with chronic salivary obstruction (**b**) from a right submandibular duct stone (*black arrow*) has atrophy of the right submandibular gland and replacement of the space with dark fatty tissue. The left submandibular gland is visible (*white arrowhead*), whereas the right gland appears to be absent although the patient has never had surgical removal

and infection of the salivary glands for potential abscess formation. Small calculi are best seen with non-contrast CT (Fig. 2.4a) and when found along the course of the parotid or submandibular ducts can diagnose the source of recurrent gland inflammation. Calcifications can also be found within certain tumors such as pleomorphic adenoma, Warthin's tumor, acinic cell carcinoma, and adenoid cystic carcinoma. Chronic inflammation and obstruction can lead to atrophy and fatty replacement of the gland (Fig. 2.4b). For malignant lesions of the salivary glands, CT images can assess invasion of adjacent bone such as the temporal bone, mandible, hard palate, and skull base. Diffuse punctate microcalcifications within the salivary gland parenchyma typically represent chronic inflammation that can be from Sjogren's syndrome, autoimmune disorders, or tuberculosis. Multiple linear calcifications may represent phleboliths within vascular malformations associated with the masseter or parotid gland.

Disadvantages of CT imaging include poor visualization of the dilated salivary duct and contraindications for contrast in those with impaired renal function and history of allergic reaction to iodine-based contrast. Streak artifacts from dental fillings can obscure pathology. CT involves exposure to ionizing radiation; specifically, the median effective dose for a neck CT with contrast is 4 mSv (millisieverts) which is the equivalent of 55 conventional chest radiographs. The importance and effects of lifetime radiation exposure are gaining attention and requires further study [6].

Magnetic Resonance Imaging (MRI)

MRI produces excellent soft-tissue contrast and resolution and is the superior imaging modality for evaluating masses and tumors of the salivary glands. Unlike CT, MRI does not involve ionizing radiation. Common MR sequences to evaluate the salivary glands include T1 weighted, T2 weighted, and T1 weighted with gadolinium contrast and fat-saturation images. MRI can also provide information about perineural invasion, tumor margins, extent of involvement in the parapharyngeal space, and lymph node metastasis. MRI offers the best visualization of the facial nerve which can sometimes be seen traversing the fat pad near the stylomastoid foramen. The plane of the nerve within the parotid gland is estimated using the stylomastoid foramen and the retromandibular vein. MR has limited abilities to detect calcifications but is superior for demonstrating tumor margins, perineural tumor spread, and intracranial invasion [7].

MRI disadvantages include high cost and longer scan time required. Patients with certain metallic implants and pacemakers cannot enter the scanner, and those with claustrophobia can have difficulty tolerating the scanner for long periods of time.

Sialography

Historically, sialography has been the main diagnostic method for sialolithiasis and salivary obstruction dating back to 1902 [7]. Sialography provides visualization of the main salivary duct and all its branches within the gland parenchyma. Sialography technique involves cannulation of Stensen's or Wharton's ducts and infusion of contrast material to outline duct anatomy. In digital subtraction sialography, an X-ray image is taken prior to contrast infusion and subtracted from post-contrast images. A sialogogue is then administered to promote the gland to empty and excrete the contrast, and afterward, a post-excretion scan demonstrates contrast clearance or retention. Examination of the ducts for filling defects, strictures, or overall size can aid in diagnosis of chronic obstructive symptoms [8].

Sialography is contraindicated in acute inflammatory conditions due to the risk for duct injury and exacerbation of infection. A successful sialogram depends on skilled cannulation of the salivary duct papillae and careful infusion of contrast. The duct dilation required for contrast application has potential therapeutic effects. Sialography is currently reserved for evaluation of obstructive and inflammatory conditions as it has limited abilities to image tumors within the glands. Disadvantages of conventional sialography include its invasive nature compared to other imaging modalities and limitations due to the use of static X-ray images. In many institutions sialography has been replaced by ultrasound or multi-planar imaging followed by therapeutic sialendoscopy. However, in certain cases detailed anatomy of the duct system is desired. For example, sialography can provide evaluation of salivary ducts after sialodochoplasty and assessment of sialectasis and salivary duct stenosis (Fig. 2.5).

MR sialography is a newer MRI protocol to image the salivary ducts using heavily T2-weighted

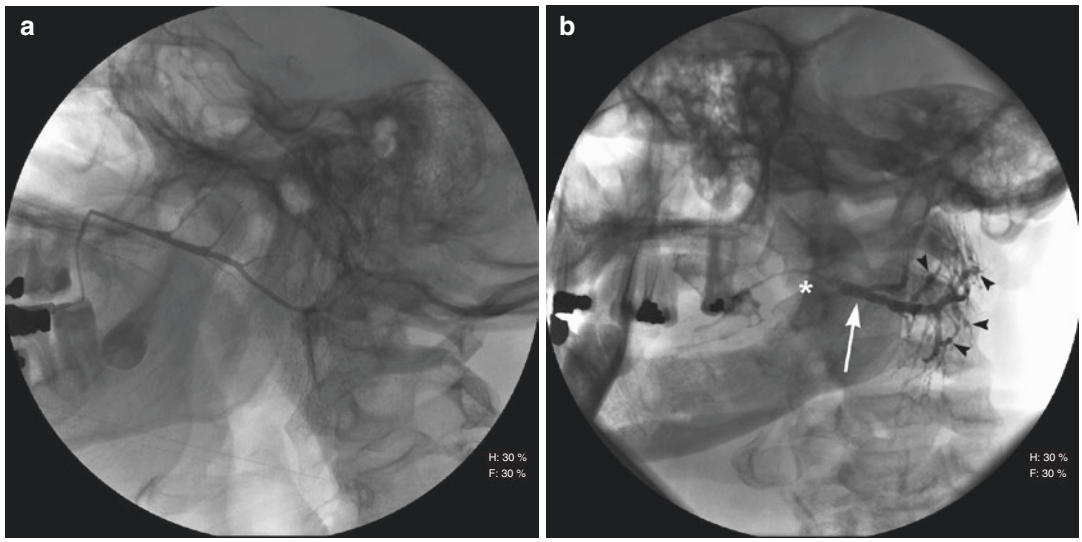

Fig. 2.5 A normal left parotid sialogram has smooth duct contour and visualization of multiple duct branches after contrast injection (**a**). In comparison, a left distal parotid duct stricture (**b**) is demonstrated with restricted duct size (*) and proximal duct dilation (*white arrow*). The intraglandular parotid ducts display sialectasis as shown by the irregular beaded appearance (*black arrowheads*). The findings of irregular main duct contour, dilated proximal ducts, and degeneration in the gland are seen in chronic sialadenitis from parotid duct stenosis. Sialogram figures courtesy of Hoffman HT, Iowa head and neck protocols

imaging protocol that does not require cannulation of the salivary duct and does not expose patients to radiation. MR sialography has been demonstrated to be effective in evaluating calculi and duct stenoses with limitations for calculi smaller than 3 mm without dilated ducts [9]. The abilities of MR sialography to detect duct dilation, calculi, and stenoses are comparable to US and conventional sialography [9]. However, the spatial resolution of secondary and tertiary branches on MR sialography is not as clearly visualized as with conventional sialography. A standard MR sialography protocol has not been established and multiple approaches have been described [10].

Salivary Scintigraphy

Salivary gland scintigraphy is a nuclear medicine study performed to examine salivary gland function in Sjogren's syndrome and after external beam or radioactive iodine radiation therapy. Techniques for salivary scintigraphy were developed to measure salivary gland hypofunction. Patients are given intravenous ^{99m}Tc-pertechnetate, and a gamma camera is used to image the gland and quantify radioactivity (counts/second). Afterward, patients are administered a sialogogue to stimulate salivary excretion, and rate of excretion is measured [11]. Patients with Sjogren's syndrome can demonstrate decreased uptake and decreased excretion of the pertechnetate from the salivary glands. Radiation treatment such as 131I for thyroid ablation can also cause functional salivary gland impairment. Overall, guidelines and consensus on scintigraphy protocols are lacking, making interpretation and comparison between institutions and studies challenging.

Imaging of Specific Salivary Conditions

Salivary Gland Neoplasms

Imaging is used to demonstrate tumor location in the superficial or deep lobe of the parotid and determine extraglandular extension, invasion of surrounding tissues, and nodal metastasis. US can be used initially to establish location of superficial lesions and obtain US-guided fine-needle aspiration biopsy for diagnosis. If the pathology is non-diagnostic or malignant or more detailed cross-sectional assessment is desired, MRI is typically the next step.

Pleomorphic Adenoma

Pleomorphic adenomas are the most common benign salivary gland tumor. They typically have smooth borders and rounded appearance with lobulations on imaging. On US the pleomorphic adenoma is typically hypoechoic with posterior acoustic enhancement. On MRI lesions display low signal intensity on T1 and intermediate to high signal intensity on T2-weighted images and can enhance with gadolinium (Fig. 2.6). Lesions can be homogeneous or heterogeneous when the larger tumors have internal cystic changes [4]. Signal intensity can vary with areas of internal hemorrhage in the tumor. On CT pleomorphic adenomas appear as smooth, ovoid, enhancing masses, occasionally with internal calcifications. Lesions that widen the stylomandibular space and displace the parapharyngeal fat suggest involvement of the deep parotid lobe.

Warthin Tumor (Papillary Cystadenoma Lymphomatosum)

Warthin tumors can occur bilaterally and are often multifocal in the parotid glands. These tumors are well-defined lesions that most commonly occur in the parotid tail. Lesions can have both cystic and solid components, occasionally with septations. On ultrasound the lesions appear as well-defined masses with multiple anechoic areas. On MRI, Warthin tumors have intermediate signal on T1 and intermediate signal intensity with focal hyperintense areas on T2 images [4]. These lesions can have minimal to no contrast enhancement and appear heterogeneous due to multiple internal components.

Malignant Tumors

Common malignant lesions of the salivary gland include mucoepidermoid carcinoma, adenoid cystic carcinoma, acinic cell carcinoma, carcinoma ex pleomorphic adenoma,

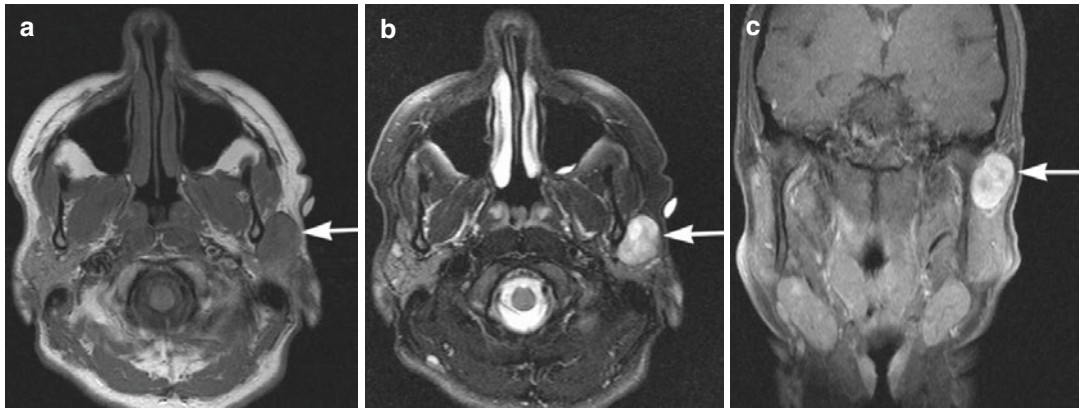

Fig. 2.6 MR images from the same patient with pleomorphic adenoma show a left parotid lesion (*arrows*) with low signal intensity on T1-weighted axial image (**a**), well-circumscribed high signal intensity on T2-weighted axial image (**b**), and heterogeneous enhancement with contrast on T1 coronal image with contrast and fat saturation (**c**)

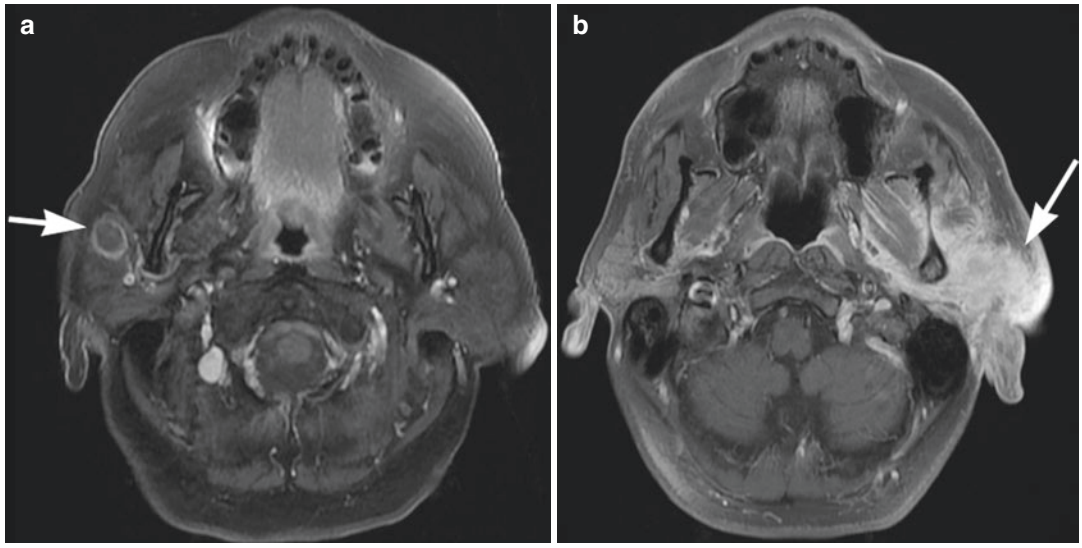

Fig. 2.7 T1-weighted MR images show right intraparotid lesion (**a**) of low intensity and surrounding contrast enhancement (*arrow*) in a patient with metastatic squamous cell carcinoma. A left parotid adenocarcinoma (**b**, *arrow*) has irregular borders and bright contrast enhancement and demonstrates involvement of the superficial and deep parotid lobes

salivary duct carcinoma, metastatic squamous cell carcinoma or melanoma, and non-Hodgkin's lymphoma. Low-grade tumors can be hard to distinguish from benign tumors since both present as well-circumscribed lesions. Features that suggest high-grade or aggressive malignancies include ill-defined masses with invasive features and metastatic lymphadenopathy (Fig. 2.7). On MRI high-grade lesions with more cellularity can be represented with low signal intensity on both T1- and T2-weighted sequences. Replacement of the fat in the stylomastoid foramen or enhancement of the mastoid segment of the facial nerve suggests perineural invasion. Large deep-lobe tumors can exhibit extension along the auriculotemporal nerve up to the foramen ovale (V3). CT imaging can aid in assessing the extent of skull base and mandible bony invasion. Multifocal disease is suggestive of parotid nodal metastases from the face, scalp, or ear skin, or lymphoma. Metastatic disease and lymphoma can

present in the parotid gland due to the presence of intraglandular parotid lymph nodes that are not found in submandibular or sublingual glands. Further evaluation with PET nuclear medicine studies can be considered in cases with suspected metastases.

Lymphoepithelial Cysts

Lymphoepithelial cysts appear as multiple mixed cystic and solid lesions usually in the parotid gland. Lesions are well-circumscribed, hypodense cysts on CT. On MRI lesions have low signal intensity on T1 and hyperintensity on T2-weighted images. Solid lesions can enhance with contrast or appear heterogeneous. On US lesions can appear as simple cysts or as mixed masses with solid components. Cysts can have thin septations and 40% have mural nodules [4]. Active HIV disease is associated with lymphoepithelial cyst formation and additionally can present with tissue hypertrophy of the palatine tonsils, lingual tonsils, and adenoids.

Salivary Gland Inflammation and Obstruction

Acute Inflammation

Acute sialadenitis is defined by acute swelling and pain over a major salivary gland. Bacterial sialadenitis is typically unilateral and presents with diffuse inflammation of the gland and overlying soft tissues. Viral sialadenitis can commonly involve bilateral parotid glands. Imaging with contrast-enhanced CT or US can be done to evaluate for infectious sequelae such as abscesses. CT imaging will demonstrate an enlarged gland with inflammatory stranding in the overlying soft tissues and strong enhancement with contrast (Fig. 2.8). Abscesses, if present, will appear as rim-enhancing lesions with internal decreased intensity. Abscess size, location, and extent on imaging can help define need for further intervention. On US the infected gland appears hypoechoic and heterogeneous. Focal hypoechoic collections suggest abscess

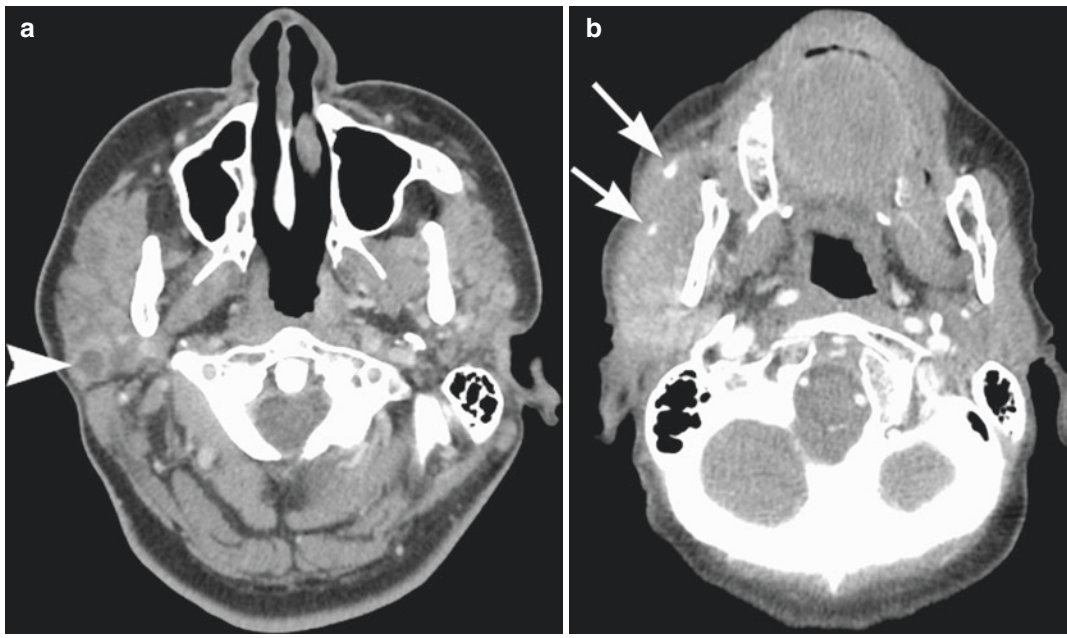

Fig. 2.8 CT scan with right acute parotid sialadenitis (**a**) with enlargement of the gland and a small rim-enhancing hypointense collection indicating an early abscess (*arrowhead*). The left parotid shows heterogeneous fatty replacement consistent with chronic immune-mediated inflammation from Sjogren's syndrome. Right acute parotid inflammation with obstruction from two parotid duct stones (**b**, *arrows*)

formation, and US guidance may be used for aspiration. Evaluation for calculi that may have caused salivary flow obstruction can be done with CT or US; however, acute inflammation and pain may limit a full US exam requiring a repeat study once the acute infection has been managed.

Sialolithiasis

Salivary duct calculi present more commonly in the submandibular gland system (80%) compared to the parotid gland (20%). The submandibular gland produces relatively more viscous saliva with higher concentration of hydroxyapatites and phosphates [1]. Wharton's duct also has a narrower papilla, and the duct location and ascent from the inferiorly positioned gland to the papilla in the anterior floor of mouth are more conducive to saliva retention and stasis. The most common site for Wharton's duct stone formation and impaction, seen in 53% of cases, is in the proximal duct near the hilum of the gland where the duct bends around the posterior border of the mylohyoid, sometimes referred to as the "comma" region of the duct. Other submandibular calculi are located in the mid-portion of the duct and near the papilla in the anterior floor of mouth (37%). Parotid duct calculi are most commonly found in the distal main Stensen's duct compared to the hilum of the gland [12].

Salivary duct calcifications can almost always be visualized with a fine-cut CT scan without contrast. If contrast is used for other purposes, the image should be windowed appropriately to visualize calcified tissue. Images should be carefully reviewed to examine the entire course of the submandibular and parotid ducts. Calculi near the anterior floor of mouth can be missed upon initial review especially in the setting of acute sialadenitis and infection (Fig. 2.9). Alternatively, calcifications within other tissues such as the tonsils can also be confused for salivary stones. US can detect most calculi larger than 2 mm. Smaller calcifications fail to exhibit posterior acoustic shadows. Bimanual sono-palpation helps with visualization of the most distal portions of the parotid and submandibular ducts. MRI and MR sialography depend on visualization of the salivary ducts on T2-weighted or contrast-enhanced images. Sialoliths are then detected by the presence of a flow void inside the duct (Fig. 2.10).

Fig. 2.9 CT scan without contrast demonstrates a small calcification (*black arrowhead*) in the right anterior floor of mouth that was missed on the formal radiographic report. Evaluation of the full course of the submandibular gland and duct is necessary to evaluate for sialolithiasis

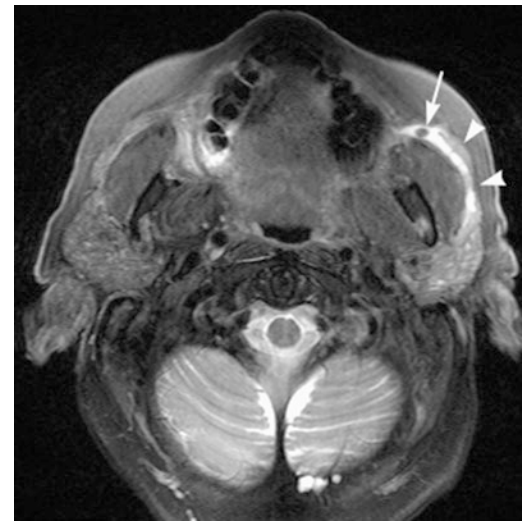

Fig. 2.10 T2-weighted MRI scan allows visualization of salivary stasis within a dilated left parotid duct (*arrowheads*). The distal portion of the duct is obstructed with a salivary stone (*arrow*) that can be seen when surrounding by the hyperintense saliva within the duct

The location of a calculus on imaging helps with surgical planning and preoperative counseling. Parotid duct calculi located in the proximal gland posterior to the masseter muscle are difficult to visualize on sialendoscopy, and many of these patients may require a combined approach with transfacial incision for management of calculi in this location. Calculi found near the parotid papilla distal to the anterior masseter border can be managed with endoscopic techniques or through transoral sialodochotomy for removal through a small incision in the buccal mucosa [2].

Chronic Sialadenitis from Autoimmune and Granulomatous Disease

The most common autoimmune disease to affect the salivary glands is Sjogren's syndrome. Sjogren's syndrome causes destruction of salivary gland parenchyma. Imaging can reveal bilateral and multiple cystic and solid lesions, making the parenchyma appear heterogeneous (Fig. 2.11a). Cystic degeneration reflects tissue destruction and solid masses represent lymphocyte aggregates. The glands can also display abnormally increased fat deposition and multiple punctate calcifications [13]. US will demonstrate bilateral parotids that appear heterogeneous with hypoechoic lesions and prominent intraparotid lymph nodes. CT imaging can reveal multiple punctate calcifications within the gland that should not be confused with larger salivary duct sialoliths (Fig. 2.11b). MR imaging displays diffuse high-intensity T2 foci within the gland. Sialography is sensitive to diagnosis of Sjogren's syndrome displaying punctate sialectasis (Fig. 2.11c) progressing to globular and cavitary parotid duct changes with more advanced disease [13]. Risk for malignant transformation to non-Hodgkin's lymphoma in the gland is 16- to 40-fold higher in patients with Sjogren's syndrome so annual monitoring is recommended and can be done with ultrasound. The 2002 American-European Consensus Group classification criteria for Sjogren's syndrome describes the use of three possible measures of salivary gland hypofunction: (1) unstimulated whole salivary flow (<1.5 ml in 15 min); (2) parotid sialography showing diffuse sialectasis; or (3) salivary scintigraphy showing delayed uptake, reduced concentration, and/or delayed excretion of tracer [14]. Since then the use of ultrasound to examine for signs of salivary gland degeneration is as effective as sialography in differentiating between patients with and without Sjogren's syndrome [15]. The current American College of Rheumatology classification for Sjogren's syndrome includes three objective measures for diagnosis using (1) lymphocytic infiltrates in lip biopsy specimens, (2) serum testing for anti-SSA and/or SSB antibodies or ANA and RF, and (3) ocular staining test. The use of US as an alternative third ACR classification item yielded similar sensitivity and specificity to the original classification suggesting that US may useful in place of other more invasive tests [16].

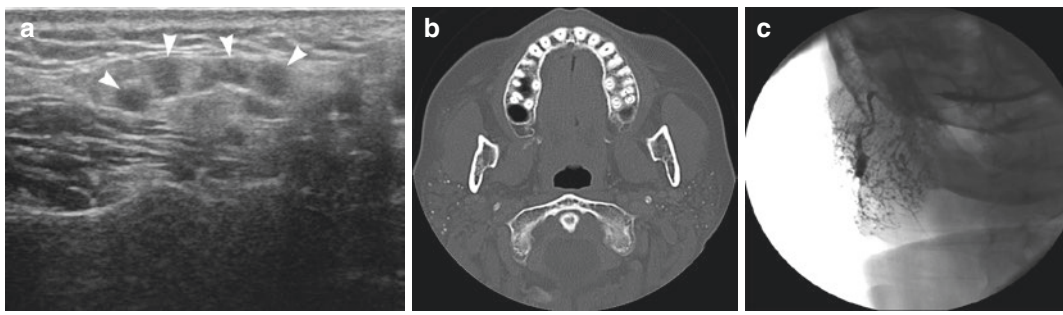

Fig. 2.11 Chronic sialadenitis from Sjogren's syndrome manifests with parotid degeneration: heterogeneous parenchyma with multiple hypoechoic areas on US (**a**), multiple punctate calcifications with the gland (**b**), and dilated acini with ductal strictures that appear as multiple areas of contrast collection on sialography (**c**). Sialogram figure courtesy of Hoffman HT, Iowa Head and Neck Protocols

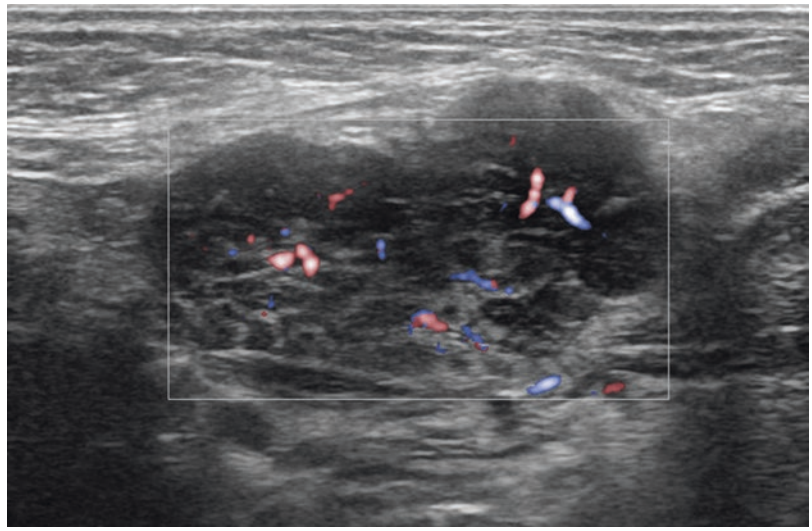

Fig. 2.12 Ultrasound image of the right submandibular gland in a patient with IgG4-related sialadenitis with enlarged and firm bilateral submandibular glands. The gland demonstrates heterogeneity, enlargement, and hypervascularity. No tumor or lesions were found within the gland, and the patient was treated with an oral steroid regimen

Other chronic immune-mediated and granulomatous diseases can mimic the gland heterogeneity seen in Sjogren's syndrome: sarcoidosis, HIV infection, lymphoma, juvenile recurrent parotitis, and IgG4-related sialadenitis (formerly Mikulicz's disease or Kuttner's tumor) (Fig. 2.12). Clinical differentiation with symptoms and laboratory testing is still necessary to distinguish between these disease entities.

Stenosis

Salivary duct stenosis can be demonstrated on US as dilated salivary ducts without intraductal obstructive calculi. A dilated main parotid duct can be visualized in the transverse plane running over the masseter muscle (Fig. 2.2a). Stenosis can be idiopathic or associated with immune-mediated salivary disease, prior radioactive iodine treatment, trauma, or mechanical obstruction from masseter hypertrophy with kinking of the parotid duct. Longstanding focal stenoses of the papilla can lead to significant salivary duct dilation (Fig. 2.2a). Sialography can also demonstrate the location and length of stenoses (Fig. 2.5). Distal duct stenosis can be dilated using progressive dilators or sialendoscopy. Intraoperative ultrasound guidance can confirm instrument placement within the salivary duct [17].

Chronic sialadenitis from long-term stenotic obstruction or autoimmune disease leads to changes in the gland parenchyma. The gland tissue becomes heterogeneous with scattered hypoechoic areas that represent degenerative salivary tissue, lymphoid tissue infiltration, and dilated salivary ducts [3]. Multiple microcalcifications within the parenchyma of the gland also represent this inflammatory process and should not be confused for intraductal calculi (Fig. 2.11b). End-stage inflammatory or post-radiation disease produces an atrophic gland with minimal salivary output.

References

1. Rzymska-Grala I, Stopa Z, Grala B, Golebiowski M, Wanyura H, Zuchowska A, et al. Salivary gland calculi—contemporary methods of imaging. Pol J Radiol. 2010;75(3):25–37.
2. Kiringoda R, Eisele DW, Chang JL. A comparison of parotid imaging characteristics and sialendoscopic findings in obstructive salivary disorders. Laryngoscope. 2014;124(12):2696–701. doi:10.1002/lary.24787.
3. Jecker P, Orloff LA. Salivary gland ultrasonography. In: Orloff LA, editor. Head and neck ultrasonography. San Diego: Plural Publishing; 2008. p. 129–52.
4. Harnsberger HR, Glastonbury CM. Parotid space. In: Harnsberger HR, editor. Diagnostic imaging: head and neck. Salt Lake: Amirsys; 2004. Section 7. p. 2–36.
5. Gritzmann N, Rettenbacher T, Hollerweger A, Macheiner P, Hubner E. Sonography of the salivary glands. Eur Radiol. 2003;13(5):964–75.
6. Smith-Bindman R, Lipson J, Marcus R, Kim KP, Mahesh M, Gould R, et al. Radiation dose associated with common computed tomography examinations and the associated lifetime attributable risk of cancer. Arch Intern Med. 2009;169(22):2078–86. doi:10.1001/archinternmed.2009.427.

7. Afzelius P, Nielsen MY, Ewertsen C, Boch KP. Imaging of the major salivary glands. Clin Physiol Funct Imaging. 2016;36(1):1–10. doi:10.1111/cpf.12199.
8. Hoffman HT (editor). Sialograms and sialography. In: Iowa head and neck protocols. 2015. https://iowa-headneckprotocols.oto.uiowa.edu/display/protocols/Sialograms+and+Sialography. Accessed 18 Mar 2016.
9. Becker M, Marchal F, Becker CD, Dulguerov P, Georgakopoulos G, Lehmann W, et al. Sialolithiasis and salivary ductal stenosis: diagnostic accuracy of MR sialography with a three-dimensional extended-phase conjugate-symmetry rapid spin-echo sequence. Radiology. 2000;217(2):347–58.
10. Jager L, Menaer F, Holzknecht N, Scholz V, Grevers G, Reiser M. Sialolithiasis: MR sialography of the submandibular duct – an alternative to conventional sialography and US? Radiology. 2000;216(3):665–71.
11. Shizukuishi K, Nagaoka S, Kinno Y, Saito M, Takahashi N, Kawamoto M, et al. Scoring analysis of salivary gland scintigraphy in patients with Sjogren's syndrome. Ann Nucl Med. 2003;17(8):627–31.
12. Sigismund PE, Zenk J, Koch M, et al. Nearly 3,000 salivary stones: some clinical and epidemiologic aspects. Laryngoscope. 2015;125(8):1879–82. doi:10.1002/lary.25377.
13. Sun Z, Zhang Z, Fu K, Zhao Y, Liu D, Ma Z. Diagnostic accuracy of parotid CT for identifying Sjogren's syndrome. Eur J Radiol. 2010;81(10):2702–9. doi:10.1016/j.ejrad.2011.12.034.
14. Vitali C, Bombardieri S, Jonsson R, et al. Classification criteria for Sjögren's syndrome: a revised version of the European criteria proposed by the American-European Consensus Group. Ann Rheum Dis. 2002;61:664–558.
15. Yonetsu K, Takagi Y, Sumi M, Eguchi K, Nakamura T. Sonography as a replacement for sialography for the diagnosis of salivary glands affected by Sjogren's syndrome. Ann Rheum Dis. 2002;61:276–7.
16. Takagi Y, Sumi M, Nakamura H, Iwamoto N, Horai Y, Kawakami A, Nakamura T. Ultrasounography as an additional item in the American College of Rheumatology classification of Sjogren's syndrome. Rheumatology. 2014;53(11):1977–83. doi:10.1093/rheumatology/keu238.
17. Ryan WR, Chang JL, Eisele DW. Surgeon-performed ultrasound and transfacial sialoendoscopy for complete parotid duct stenosis. Laryngoscope. 2014;124(2):418–20. doi:10.1002/lary.23968.